



1 Aqueous Reactions of Organic Triplet Excited States with Atmospheric

2 Alkenes

3 Richie Kaur ^{a,b}, Brandi M. Hudson ^c, Joseph Draper ^{a, #}, Dean J. Tantillo ^c, and Cort Anastasio ^{*a,b}

4 ^a Department of Land, Air, and Water Resources, University of California, Davis, California
5 95616, United States

6 ^b Agricultural & Environmental Chemistry Graduate Group, University of California, Davis

7 ^c Department of Chemistry, University of California, Davis, California 95616, United States

8 [#] Now at the Fresno Metropolitan Flood Control District, Fresno, California 93727, United
9 States

10 Correspondence to: C. Anastasio (canastasio@ucdavis.edu)

11

12 Abstract

13 Triplet excited states of organic matter, a.k.a. “triplets”, are formed when brown carbon absorbs
14 light. While triplets can be important photooxidants in atmospheric drops and particles (e.g., they
15 rapidly oxidize phenols), very little is known about their reactivity toward many classes of
16 organic compounds in the atmosphere. Here we measure the bimolecular rate constants of the
17 triplet excited state of benzophenone (³BP*), a model species, with 17 water-soluble C₃–C₆
18 alkenes that have either been found in the atmosphere or are reasonable surrogates for identified
19 species. Measured rate constants ($k_{\text{ALK}+3\text{BP}^*}$) vary by a factor of 30 and are in the range of (0.24 –
20 $7.5) \times 10^9 \text{ M}^{-1} \text{ s}^{-1}$. Biogenic alkenes found in the atmosphere – e.g., cis-3-hexen-1-ol, cis-3-
21 hexenyl acetate, and methyl jasmonate – react rapidly, with rate constants above $1 \times 10^9 \text{ M}^{-1} \text{ s}^{-1}$.
22 Rate constants depend on alkene characteristics such as the location of the double bond,
23 stereochemistry, and alkyl substitution on the double bond. There is a reasonable correlation
24 between $k_{\text{ALK}+3\text{BP}^*}$ and the calculated one-electron oxidation potential (OP) of the alkenes ($R^2 =$
25 0.58); in contrast, rate constants are not correlated with bond dissociation enthalpies, bond
26 dissociation free energies, or computed energy barriers for hydrogen abstraction. Using the OP
27 relationship, we estimate aqueous rate constants for a number of unsaturated isoprene and



28 limonene oxidation products with $^3\text{BP}^*$: values are in the range of $(0.080\text{--}1.7) \times 10^9 \text{ M}^{-1} \text{ s}^{-1}$,
29 with generally faster values for limonene products. Using our predicted rate constants, along
30 with values for other reactions from the literature, we conclude that triplets are probably minor
31 oxidants for isoprene and limonene-related compounds in cloudy or foggy atmospheres, except
32 in cases where the triplets are very reactive.

33

34 **1 Introduction**

35 Photochemical processes in atmospheric aqueous phases (e.g., cloud and fog drops and
36 aqueous particles) are important sources and sinks of secondary organic species (Blando and
37 Turpin, 2000; Lim et al., 2010; Kroll and Seinfeld, 2008; Volkamer et al., 2009; Gelencsér and
38 Varga, 2005), which represent a large fraction of aerosol mass (Zhang et al., 2007; Hallquist et
39 al., 2009). Many of these reactions involve photooxidants, including hydroxyl radical ($\bullet\text{OH}$),
40 which is widely considered to be the dominant aqueous oxidant (Herrmann et al., 2010;
41 Herrmann et al., 2015). But there are numerous other aqueous photooxidants, such as singlet
42 molecular oxygen, hydroperoxyl radical/superoxide radical anion, hydrogen peroxide, and triplet
43 excited states of organic matter ($^3\text{C}^*$ or triplets) (Lee et al., 2011; Anastasio and McGregor,
44 2001; Kaur and Anastasio, 2017; Anastasio et al., 1996; Anastasio et al., 1994; Zepp et al., 1977;
45 Wilkinson et al., 1995; Kaur and Anastasio, 2018). Formed from the photoexcitation of colored
46 organic matter (i.e., brown carbon), triplets are important oxidants in surface waters for several
47 classes of organic compounds, including phenols, anilines, amines, phenylurea herbicides, and
48 heterocyclic sulfur-containing compounds (Canonica et al., 1995; Canonica and Hoigné, 1995;
49 Arnold, 2014; Canonica et al., 2006a; Bahn Müller et al., 2014; Boreen et al., 2005); however,
50 very little is known about atmospheric triplets.



51 Recent studies have shown that aqueous triplets can be the dominant oxidants for phenols
52 emitted during biomass combustion (Smith et al., 2014), with phenol lifetimes on the order of a
53 few hours in fog drops (Kaur and Anastasio, 2018) and aqueous particle extracts (Kaur et al.,
54 2018). There is also evidence that triplets can oxidize some unsaturated aliphatic compounds.
55 Richards-Henderson et. al. (Richards-Henderson et al., 2014b) measured rate constants for five
56 unsaturated biogenic volatile organic compounds (BVOCs) with the model triplets 3,4-
57 dimethoxybenzaldehyde and 3'-methoxyacetophenone, and found that rate constants ranged
58 between 10^7 and $10^9 \text{ M}^{-1} \text{ s}^{-1}$. Other laboratory studies have shown that triplet states of
59 photosensitizers such as imidazole-2-carboxaldehyde and 4-benzoylbenzoic acid can oxidize
60 gaseous aliphatic BVOCs, e.g., isoprene and limonene, and model aliphatic compounds, e.g., 1-
61 octanol, at the air-water interface to form low-volatility products that increase particle mass (Fu
62 et al., 2015; Rossignol et al., 2014; Li et al., 2016; Laskin et al., 2015). However, the
63 atmospheric importance of these types of processes are unclear (Tsui et al., 2017). Additionally,
64 we recently reported that natural triplets in illuminated fog waters and particle extracts are
65 significant oxidants for methyl jasmonate, an unsaturated aliphatic BVOC, accounting for 30–80
66 % of its aqueous loss during illumination (Kaur et al., 2018; Kaur and Anastasio, 2018).

67 Abundant BVOCs such as isoprene and limonene are rapidly oxidized in the gas phase to
68 form unsaturated C_3 – C_6 oxygenated volatile organic compounds (OVOCs) that include isoprene
69 hydroxyhydroperoxides, isoprene hydroxynitrates, and isoprene and limonene aldehydes (Surratt
70 et al., 2006; Paulot et al., 2009b; Crouse et al., 2011; Ng et al., 2008; Walser et al., 2008; Paulot
71 et al., 2009a). Several of these first-generation products have high Henry's law constants, above
72 10^4 M atm^{-1} (Marais et al., 2016) and partition significantly into cloud and fog drops and, to a
73 smaller extent, into aerosol liquid water. There, they can undergo further oxidation by aqueous
74 photooxidants, including $\cdot\text{OH}$ and ozone (Wolfe et al., 2012; St. Clair et al., 2015; Khamaganov
75 and Hites, 2001; Schöne and Herrmann, 2014; Lee et al., 2014) and possibly triplets. Our past



76 measurements have shown that steady-state concentrations of $^3\text{C}^*$ are orders of magnitude higher
77 than $^{\bullet}\text{OH}$ in fog waters and aqueous particles (Kaur et al., 2018; Kaur and Anastasio, 2018) and
78 thus they might contribute significantly to the loss of OVOCs derived from isoprene and other
79 precursors. However, testing this hypothesis requires rate constants for the reactions of triplets
80 with alkenes, which are scarce.

81 To address this gap, we studied the reactions of 17 $\text{C}_3 - \text{C}_6$ unsaturated compounds with
82 the triplet state of the model compound benzophenone (Fig. 1). While our 17 unsaturated
83 compounds include alcohols, esters, and chlorinated compounds, for simplicity we refer to them
84 all as “alkenes”. The tested alkenes include BVOCs emitted into the atmosphere as well as
85 surrogates for some of the small unsaturated gas-phase products formed as secondary OVOCs.
86 The goals of this study are to: 1) measure rate constants for reactions of the alkenes with the
87 triplet excited state of benzophenone, 2) explore quantitative structure-activity relationships
88 (QSARs) between the measured rate constants and calculated alkene properties (e.g., the one-
89 electron oxidation potential) and 3) use a suitable QSAR to estimate rate constants for triplets
90 with some unsaturated isoprene and limonene oxidation products to predict whether or not
91 triplets are significant oxidants for these species in cloud and fog drops.

92

93 **2 Methods**

94 **2.1 Chemicals**

95 All chemicals were purchased from Sigma-Aldrich with purities of 95 % and above, and
96 were used as received: the compound numbers, compound names, and abbreviated names are
97 listed in Table 1. All chemical solutions were prepared using purified water (Milli-Q water) from
98 a Milli-Q Plus system (Millipore; $\geq 18.2 \text{ M}\Omega \text{ cm}$) with an upstream Barnstead activated carbon



99 cartridge. The pH of each reaction solution was adjusted to 5.5 (\pm 0.2) using a 1.0 mM phosphate
100 buffer.

101 2.2 Kinetic Experiments

102 Bimolecular rate constants of the alkenes with the triplet state of benzophenone ($^3\text{BP}^*$)
103 were measured using a relative rate technique, as described in in the literature (Richards-
104 Henderson et al., 2014a; Finlayson-Pitts and Pitts Jr, 1999). The technique involves illuminating
105 a solution containing the triplet precursor (BP), a reference compound with a known second-
106 order rate constant with $^3\text{BP}^*$, and one test alkene for which the rate constant is unknown.
107 Buffered, air-saturated solutions containing 50 μM each of the reference and test compounds and
108 100 μM of BP were prepared and then 10 mL of this solution was illuminated in a stirred 2-cm,
109 air-tight quartz cuvette (Spectrocell) at 25 $^\circ\text{C}$. Samples were illuminated with a 1000 W Xenon
110 arc lamp filtered with an AM 1.0 air mass filter (AM1D-3L, Sciencetech) and 295 nm long-pass
111 filter (20CGA-295, Thorlabs) to mimic tropospheric solar light (Fig. S1 of the Supplemental
112 Information). At various intervals, aliquots of illuminated sample were removed and analyzed for
113 the concentration of reference compound and test alkene using HPLC (Shimadzu LC-10AT
114 pump, ThermoScientific BetaBasic-18 C_{18} column (250 \times 33 mm, 5 μM bead), and Shimadzu-
115 10AT UV-Vis detector). Parallel dark controls were employed with every experiment using an
116 aluminum foil-wrapped cuvette containing the same solution in the illumination chamber and
117 analyzed in the same manner as the illuminated solutions.

118 In every case, loss of test and reference compounds followed first-order kinetics. Plotting
119 the change in concentration of the test alkene against that of the reference compound yields a
120 linear plot that is represented by:

$$121 \ln \frac{[\text{Reference}]_0}{[\text{Reference}]_t} = \frac{k_{\text{Reference} + 3\text{BP}^*}}{k_{\text{ALK} + 3\text{BP}^*}} \ln \frac{[\text{ALK}]_0}{[\text{ALK}]_t} \quad (1)$$



122 where $[\text{Reference}]_0$, $[\text{Reference}]_t$, $[\text{ALK}]_0$, and $[\text{ALK}]_t$ are the concentrations of the reference
123 and test alkenes at times zero and t , respectively, and $k_{\text{Reference}+3\text{BP}^*}$ and $k_{\text{ALK}+3\text{BP}^*}$ are the
124 bimolecular rate constants for the reaction of the reference and test alkenes with $^3\text{BP}^*$,
125 respectively. A plot of Eq. (1) (with the y-intercept fixed at the origin) gives a slope equal to the
126 ratio of the bimolecular rate constants; dividing $k_{\text{Reference}+3\text{BP}^*}$ by the slope gives $k_{\text{ALK}+3\text{BP}^*}$. The
127 measurement technique is illustrated in Fig. S2.

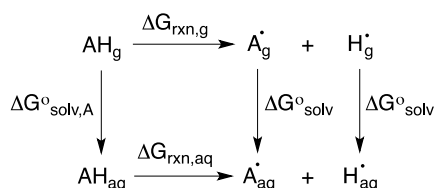
128 2.3 Calculation of Oxidation Predictor Variables

129 All calculations were completed using the Gaussian 09 software suite (Frisch et al.,
130 2009). Structures of alkenes were optimized using uB3LYP/6-31+G(d,p) (Becke, 1992, 1993;
131 Lee et al., 1988; Stephens et al., 1994; Tirado-Rives and Jorgensen, 2008) for reaction coordinate
132 calculations and the CBS-QB3 (Montgomery Jr et al., 1999) method for predicting bond
133 dissociation enthalpies (BDEs), bond dissociation free energies (BDFEs), and oxidation
134 potentials (OPs). Transition state structures (TSSs) were optimized in the triplet state using
135 uB3LYP/6-31+G(d,p) (Becke, 1992, 1993; Lee et al., 1988; Stephens et al., 1994; Tirado-Rives
136 and Jorgensen, 2008). TSSs were confirmed by the presence of an imaginary frequency and
137 minima (reactants and products) were confirmed by the absence of imaginary frequencies. Free
138 energy (ΔG) and enthalpy (ΔH) differences were determined by comparing TSS energies relative
139 to their reactant energies. For solvent phase calculations, the solvent model density (SMD)
140 (Marenich et al., 2009) continuum model was used with water as the solvent. To calculate BDEs,
141 the neutral (AH) and radical species (A^\bullet) (resulting from H atom abstraction) of each alkene and
142 the H radical (H^\bullet) were optimized in the gas phase. Using the computed enthalpies (H) and Eq.
143 (2), the predicted BDEs of each alkene were determined.

$$144 \quad BDE = H_{\text{A}^\bullet} + H_{\text{H}^\bullet} - H_{\text{AH}} \quad (2)$$



145 To determine the predicted BDFEs, the neutral (AH_g , AH_{aq}) and radical species (A^{\bullet}_g ,
 146 A^{\bullet}_{aq}) of each alkene and the H radical (H^{\bullet}_g , H^{\bullet}_{aq}) were optimized in the gas and solvent phases
 147 and their differences taken to give $\Delta G^{\circ}_{solv,AH}$, $\Delta G^{\circ}_{solv,A^{\bullet}}$, and $\Delta G^{\circ}_{solv,H^{\bullet}}$, respectively. Based on
 148 the thermodynamic cycle shown (Scheme 1), these values were used in Eqs. (3) and (4) to
 149 calculate the BDFEs of C–H and O–H bonds.

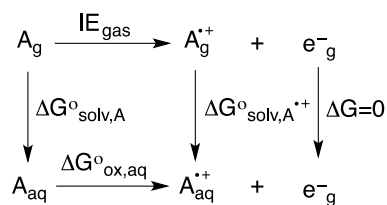


151 **Scheme 1.** Thermodynamic cycle used to calculate bond dissociation free energies.

$$152 \quad \Delta \Delta G_{solv} = \Delta G^{\circ}_{solv,A^{\bullet}} + \Delta G^{\circ}_{solv,H^{\bullet}} - \Delta G^{\circ}_{solv,AH} \quad (3)$$

$$153 \quad \Delta G^{\circ}_{ox} = \Delta G_g + \Delta \Delta G_{solv} \quad (4)$$

154 To predict OPs, the neutral (A_g , A_{aq}) and radical cation ($A^{\bullet+}_g$, $A^{\bullet+}_{aq}$) forms of each alkene
 155 were optimized in the gas and solvent phase, their difference giving $\Delta G^{\circ}_{solv,A}$ and $\Delta G^{\circ}_{solv,A^{\bullet+}}$.
 156 Based on the thermodynamic cycle shown below (Scheme 2), these values were used in Eqs. (5–
 157 7) to calculate the OP of each alkene.



159 **Scheme 2.** Thermodynamic cycle used to calculate oxidation potentials.

$$160 \quad \Delta \Delta G_{solv} = \Delta G^{\circ}_{solv,A^{\bullet+}} - \Delta G^{\circ}_{solv,A} \quad (5)$$

$$161 \quad \Delta G^{\circ}_{ox} = IE_{gas} + \Delta \Delta G_{solv} \quad (6)$$



$$162 \quad E_{ox} = -\left(\frac{-\Delta G_{ox}^{\circ}}{nF} + SHE\right) \quad (7)$$

163 where n is the number of electrons, F is Faraday's constant (96485.3365 C/mol), and SHE is the
164 potential of the standard hydrogen electrode (4.28 V).

165 Subsequent MP2/CBSB3 (Petersson et al., 1988; Petersson and Al-Laham, 1991;
166 Petersson et al., 1991; Mayer et al., 1998) single point calculations were used to compute the
167 highest occupied molecular orbitals (HOMOs) and singly occupied molecular orbitals (SOMOs).
168 Structural drawings were produced using CYLView (Legault, 2009).

169

170 **3 Results and discussion**

171 **3.1 Alkene-triplet bimolecular rate constants ($k_{\text{ALK}+3\text{BP}^*}$)**

172 Fig. 1 shows the chemical structures for all 17 alkenes and the triplet precursor,
173 benzophenone. The alkenes have molecular weights ranging between 58 and 220 g mol⁻¹ and
174 include 13 alcohols, three esters and one chlorinated compound. The model triplet precursor
175 benzophenone (BP) has been previously employed in surface water studies, and rapidly reacts
176 with aromatics such as substituted phenols and phenyl urea herbicides with rate constants faster
177 than 10⁹ M⁻¹ s⁻¹ (Canonica et al., 2000; Canonica et al., 2006b).

178 The bimolecular rate constants for the alkenes with the excited triplet state of BP
179 ($k_{\text{ALK}+3\text{BP}^*}$) vary by a factor of 30, spanning the range of (0.24–7.5) × 10⁹ M⁻¹s⁻¹. Values are
180 shown in Tables 1 and S1, and in Fig. S3, where the alkenes are numbered in ascending order of
181 their reactivity towards ³BP*. Based on their rate constants, the alkenes appear to be broadly split
182 into two groups – the slower alkenes (**1–9**), whose rate constants lie below 1 × 10⁹ M⁻¹s⁻¹ and
183 span a range of only a factor of 2.5, and the faster alkenes (**10–17**) which vary by a factor of 5.
184 Notably, three of the four BVOCs identified in emissions to the atmosphere – 3MBO (**12**), cHxO



185 (15), cHxAc (16) and MeJA (17) – react rapidly with $^3\text{BP}^*$, with rate constants greater than $1 \times$
186 $10^9 \text{ M}^{-1} \text{ s}^{-1}$.

187 Three alkene characteristics appear to increase reactivity: internal (rather than terminal)
188 double bonds; methyl substitution on the double bond; and alkene stereochemistry. To more
189 specifically examine the impact of these variables, we compare the rate constants for three sets of
190 alkenes (Fig. 2). The lowest free energy and enthalpy barriers for the abstraction of a hydrogen
191 atom are also shown in Fig. 2 (and in Table 1); while overall these computed barriers are not
192 well-correlated with rate constants (discussed below), lower barriers generally correspond to
193 higher rate constants for the sets of alkenes in Fig. 2. Based on the first two sets of compounds in
194 Fig. 2, internal alkenes react faster with $^3\text{BP}^*$ than do terminal isomers. For example, cHxAc
195 (16), an internal hexenyl acetate, has a reaction rate constant 11 times faster than its terminal
196 isomer 5HxAc (9). The corresponding alcohols also exhibit the same trend: the internal alkenes
197 cHxO (15) and tHxO (10) react 27 and 5.8 times faster, respectively, than the terminal isomer
198 5HxO (1). This dependence of reactivity on double bond location has implications for isoprene
199 hydroxyhydroperoxides (ISOPOOH) and hydroxynitrates (ISONO₂), which have both terminal
200 (β -) and non-terminal (δ -) isomers formed from gas-phase oxidation (Marais et al., 2016; Paulot
201 et al., 2009b; Paulot et al., 2009a). Based on our results we expect that the δ -isomers react more
202 quickly with organic triplets than the β -isomers.

203 Alkene stereochemistry also affects the triplet-alkene reaction rate constant. The data in
204 the middle of Fig. 2 shows that cis-HxO (15) reacts nearly five times more quickly with $^3\text{BP}^*$
205 than does trans-HxO (10), consistent with the lower predicted energy barrier for hydrogen atom
206 abstraction from the cis isomer. Finally, addition of electron-donating substituents (methyl
207 groups) on an unsaturated carbon atom also increases the rate constant. This is evident from
208 comparing 2B1O (8) and its methyl-substituted analog 3MBO (12): $k_{\text{ALK}+^3\text{BP}^*}$ is 3.7 times faster
209 with the methyl group (Fig. 2). Mechanistically, triplet-induced oxidation can proceed via either
210 hydrogen atom transfer or a proton-coupled-electron transfer (Canonica et al., 1995; Warren et



211 al., 2010; Erickson et al., 2015) and the presence of an electron-donating substituent on the
212 double bond likely selectively stabilizes the intermediates (e.g., radical or radical cation) formed
213 from these two processes, as well as the transition state structures for their formation.

214 **3.2 Relationship between k and one-electron oxidation potential**

215 Our next goal was to develop a quantitative structure-activity relationship (QSAR) so that
216 we can predict rate constants for alkene-triplet reactions. To use as predictor variables in the
217 QSARs we computed several properties of the alkenes: bond dissociation enthalpy and free
218 energy for various hydrogen atoms (Fig. S4), free energy and enthalpy barriers for hydrogen
219 atom abstraction (Table 1), and one-electron oxidation potentials (Table 1). Apart from the
220 oxidation potential, none of the other properties correlate well with the measured rate constants
221 (Figs. S5 and S6). While there is no correlation between the rate constants and predicted energy
222 barriers, alkenes with lower predicted free energy barriers (ΔG^\ddagger) are predicted to be fast-reacting,
223 with rate constants above $5 \times 10^8 \text{ M}^{-1} \text{ s}^{-1}$ (Fig. S6). As shown in Fig. S6, computed barriers
224 predict a much larger variation in rate than observed experimentally, suggesting that the breaking
225 of the C–H or O–H bond does not occur in the rate-determining step for all alkenes.

226 Of all the properties examined, the one-electron oxidation potential (OP) of the alkenes
227 best correlates with the (log of) measured rate constants, with rate constants generally increasing
228 as the alkenes are more easily oxidized, i.e., at lower OP values ($R^2 = 0.58$) (Fig. 3). Measured
229 rate constants for 13 of the 16 alkenes lie within (or very near to) the 95 % confidence interval
230 (blue lines) of the regression fit, but there are three notable outliers: hexen-1,3-diol (**3**, HDO),
231 cis-3-hexen-1-ol (**15**, cHxO) and cis-3-hexenylacetate (**16**, cHxAc). The measured HDO rate
232 constant is 3.3 times lower than that predicted by the regression line, while measured rate
233 constants for cHxO and cHxAc are 3.9 and 4.9 times higher, respectively, than predicted.

234 To try to assess why these compounds differ from the others, we calculated the highest
235 occupied molecular orbital (HOMO) of the alkene and the singly occupied molecular orbital
236 (SOMO) of the alkene radical cation (i.e., after oxidation) (Fig. 4). Depending on the system,



237 oxidation is predicted to occur by removing an electron either from the π system of the C–C
238 double bond or from a lone pair on the O atom. This is illustrated in Fig. 4, which shows the
239 HOMO and SOMO structures for HDO (**3**), where the electron is removed from the C-C double
240 bond, and 3B1O (**5**), where the electron is removed from the oxygen atom. However, the three
241 outliers in the correlation do not all fall into just one of these categories: for cHxAc (**16**) the
242 electron is most likely abstracted from the oxygen, while for HDO (**3**) and cHxO (**15**) the
243 electron is likely removed from the π system (Tables S2 and S3). This suggests that the location
244 of electron removal does not control the rate constants. We also examined if the rate of loss of
245 cHxO might be enhanced due to oligomerization, where an initially formed cHxO radical leads
246 to additional cHxO loss. Since the pseudo-first-order rate constant of oligomerization should
247 increase with initial cHxO concentration, we measured the rate constant for cHxO loss over a
248 range of initial concentrations (2–50 μM). However, as shown in Fig. S8, the rate constant for
249 cHxO loss does not depend on its concentration, suggesting that oligomerization is an
250 unimportant loss process for cHxO in our experiments. Thus, it is not clear why these three
251 compounds do not fall closer to the regression line of Fig. 3. However, except for **16**, all of the
252 alkenes fall within a factor of four of the correlation line (grey lines). Finally, even though there
253 is a good correlation between rate constant and OP in Fig. 3, it does not indicate whether these
254 reactions proceed via pure electron transfer, proton-coupled electron transfer, or hydrogen
255 transfer. As discussed earlier, since the predicted energy barriers for hydrogen abstraction do not
256 correlate with measured rate constants (Fig. S6) and appear to split into two groups, there
257 remains uncertainty about the mechanism of triplet-induced oxidation of the alkenes.

258 **3.3 Predicted triplet-OVOC bimolecular rate constants**

259 We next use the relationship in Fig. 3, along with calculated oxidation potentials, to
260 predict second-order rate constants for $^3\text{BP}^*$ with a set of unsaturated isoprene- and limonene-
261 derived OVOCs. As shown in Fig. 5, we predict that limonene products generally react faster



262 with ³BP* than do isoprene products. For the five isoprene-derived OVOCs that we considered,
263 rate constants vary by a factor of 17, and range between $(0.080\text{--}1.4) \times 10^9 \text{ M}^{-1} \text{ s}^{-1}$ (Table 1, Fig.
264 5). The δ -isomers of ISOPOOH and ISONO₂, which contain internal double bonds, have lower
265 computed one-electron oxidation potentials and thus higher predicted rate constants compared to
266 the terminal β -isomers. This is similar to the trend observed with the other alkenes (Fig. 2). In
267 case of isoprene hydroperoxyaldehydes, we were able to determine the oxidation potential for
268 only HPALD2 (**22**), and its predicted reaction rate constant (± 1 SE) of $4.0 (\pm 0.9) \times 10^8 \text{ M}^{-1} \text{ s}^{-1}$
269 is among the lowest of the isoprene-derived alkenes (Fig. 5).

270 We calculated OP values and triplet rate constants for three limonene-derived OVOCs:
271 limonene aldehyde (LMNALD) and two dihydroxy-limonene aldehydes (2,5OH-LMNALD and
272 4,7OH-LMNALD). Compared to the isoprene-derived alkenes, the rate constants for all three
273 limonene products are high, and range between $(0.89\text{--}1.7) \times 10^9 \text{ M}^{-1} \text{ s}^{-1}$. All of the limonene
274 aldehydes (as well as the isoprene products) can have several isomers whose calculated oxidation
275 potentials can vary, which affects the predicted rate constant. For example, for 4,7OH-LMNALD
276 (**25**) the computed oxidation potential for five of its isomers vary between 2.17 and 2.48 V
277 (Table S4), which leads to a relative standard deviation of 40 % in the predicted rate constants
278 for the various isomers. For each OVOC, the predicted rate constants in Table 1 are for the
279 lowest energy isomers whose structures are shown in Fig. S9.

280 **3.4 Role of triplets in the fate of isoprene- and limonene-derived OVOCs**

281 Next, we use our estimated rate constants, along with previously published estimated
282 values for rates of other loss processes (Table S5), to understand the importance of triplets as
283 sinks for isoprene- and limonene-derived OVOCs in a foggy/cloudy atmosphere. For our simple
284 calculations we use a liquid water content of $1 \times 10^{-6} \text{ L-aq/L-g}$, a temperature of 25 °C, and
285 calculated Henry's law constants from EPISuite (US EPA. Estimation Programs Interface
286 Suite™ for Microsoft® Windows v 4.1, 2016) (Table S6). From these inputs, we estimate that



287 between 10 and 97 % of the OVOCs will be partitioned into the aqueous phase under our
288 conditions (Table S6). The OVOC sinks we consider are photolysis and reactions with hydroxyl
289 radical ($\bullet\text{OH}$) and ozone (O_3) in the gas phase as well as hydrolysis and reactions with $\bullet\text{OH}$, O_3 ,
290 and triplets in the aqueous phase (Table S5). Based on typical oxidant concentrations in both
291 phases and available rate constants with sinks, the overall pseudo-first-order rate constants for
292 OVOC loss are estimated to be in the range of $(0.27\text{--}3.0) \times 10^{-4} \text{ s}^{-1}$, corresponding to overall
293 lifetimes of 0.93 to 10 h (Table S7). The only exception is δ -ISONO₂, which is expected to
294 undergo rapid hydrolysis to form its corresponding diol (Jacobs et al., 2014) with a lifetime of
295 just 0.078 h (280 s).

296 Fig. 6 shows the overall loss rate constants, and the contribution from each pathway, for
297 four of these OVOCs: δ 4-ISOPOOH (**19**), β -ISONO₂ (**20**), HPALD2 (**22**) AND 4,7-OH
298 LMNALD (**25**). Overall, aqueous-phase processes dominate the fate of these OVOCs,
299 accounting for the bulk of their loss; but the contribution of aqueous triplets to OVOC loss
300 depends strongly on the triplet reactivity. Panel (a) of Fig. 6 shows OVOC loss when we assume
301 that the aqueous triplets are highly reactive, i.e., using rate constants estimated for $^3\text{BP}^*$ (Fig. 5).
302 Since our recent measurements (Kaur et al., 2018; Kaur and Anastasio, 2018) indicate that, on
303 average, ambient triplets are not this reactive, this scenario likely represents an upper bound for
304 the triplet contribution. In this case triplets are the dominant sinks for δ 4-ISOPOOH and 4,7-OH
305 LMNALD, accounting for 74 % and 47 % of their total losses, respectively (Fig. 6a). For β -
306 ISONO₂ and HPALD2, triplets are not dominant but still significant, accounting for 19 % and 24
307 % of loss, respectively, while other sinks dominate. For the OVOCs where we calculated rate
308 constants with $^3\text{BP}^*$ (Fig. 5) but that are not shown in Fig. 6, the triplet contribution varies
309 widely, from less than 1 % for δ -ISONO₂ (**21**), where hydrolysis dominates, to 59 % for 2,5-OH
310 LMNALD (**24**) (Table S7).



311 While $^3\text{BP}^*$ likely represents an upper-bound of triplet reactivity in atmospheric waters,
312 our recent measurements indicate that the triplets in fog waters and particles have an average
313 reactivity that is typically similar to 3'-methoxyacetophenone (3MAP) and 3,4-
314 dimethoxybenzaldehyde (DMB) (Kaur et al., 2018; Kaur and Anastasio, 2018). A comparison of
315 our $^3\text{BP}^*$ rate constants (Table 1) with the average values for the 3MAP and DMB triplets for a
316 subset of the alkenes (Richards-Henderson et al., 2014b) indicates that the average 3MAP/DMB
317 triplet rate constants are 1–18 % of the corresponding $^3\text{BP}^*$ values. Thus to scale alkene-triplet
318 rate constants from $^3\text{BP}^*$ to the 3MAP and DMB triplets we take the median value of 4 %, which
319 is derived from the MeJA rate constants (Table S8). Fig. 6b shows the calculated fates of the
320 OVOCs in the case where we consider “typical reactivity” triplets, i.e., where we multiply the
321 $^3\text{BP}^*$ + OVOC rate constants (Fig. 5) by a factor of 0.04. Under these conditions, triplets are
322 minor oxidants (Fig. 6b), accounting for 9 % and 3 % of the loss of δ^4 -ISOPOOH and 4,7-
323 LMNALD, respectively, and approximately 1 % for the other two OVOCs. This suggests that
324 aqueous triplets are generally minor sinks for OVOCs derived from isoprene and limonene, in
325 contrast to the case for phenols, where triplets appear to be the major sink (Smith et al., 2014; Yu
326 et al., 2014; Kaur and Anastasio, 2018). However, there are several important uncertainties in
327 our determination that triplets are likely minor sinks for oxygenated alkenes. First, the factor we
328 used to adjust from $^3\text{BP}^*$ rate constants to triplet 3MAP/DMB rate constants (i.e., a factor of
329 0.04) is quite uncertain: values for the three BVOCs examined range from 0.01 to 0.18 (Table
330 S8). Additionally, there are very few measurements of triplets in atmospheric drops or particles
331 (Kaur et al., 2018; Kaur and Anastasio, 2018), and only from two sites, so it is possible that we
332 are underestimating the average reactivity and/or concentrations of triplets in atmospheric drops
333 and particles.



334 4 Conclusions

335 To explore whether triplet excited states of organic matter might be important sinks for
336 unsaturated organic compounds, we measured rate constants for 17 C₃–C₆ alkenes with the triplet
337 excited state of benzophenone (³BP*). The resulting bimolecular rate constants span the range of
338 $(0.24\text{--}7.5) \times 10^9 \text{ M}^{-1}\text{s}^{-1}$. Notably, the rate constants are high (above $10^9 \text{ M}^{-1}\text{s}^{-1}$) for some
339 important green leaf volatiles emitted from plants – 3MBO, cHxO, cHxAc, and MeJA. Rate
340 constants appear to be enhanced by alkene characteristics such as an internal double bond, cis-
341 stereochemistry, and alkyl substitution on the double bond.

342 To be able to predict rate constants for other alkenes, we examined QSARs between our
343 measured rate constants and a variety of calculated properties for the alkenes and ³BP*-alkene
344 transition states. Rate constants are not correlated with bond dissociation enthalpies, free
345 energies or predicted energy barriers for removal of various hydrogen atoms, but are reasonably
346 correlated with the one-electron oxidation potential of the alkenes ($R^2 = 0.58$). Based on the
347 relationship between rate constants and oxidation potential, we predict that highly reactive
348 triplets will react with first generation isoprene- and limonene- oxidation products with rate
349 constants on the order of $10^8\text{--}10^9 \text{ M}^{-1} \text{ s}^{-1}$, with higher values for the δ -isomers compared to
350 terminal β -isomer products. Using these rate constants in a simple model of OVOC chemistry in
351 a foggy/cloudy atmosphere suggests that highly reactive aqueous triplets could be significant
352 oxidants for some isoprene hydroxyhydroperoxides and limonene aldehydes. However, for our
353 current best estimate of typical reactivities, triplets are a minor sink for isoprene- and limonene-
354 derived OVOCs.

355 To more specifically quantify the contributions of triplet excited states towards the loss of
356 alkenes in particles and drops requires more insight into both the reactivities and concentrations
357 of atmospheric triplet species. In addition, assessing whether triplets might be important sinks for



358 other organic species requires more measurements of reaction rate constants with
359 atmospherically relevant organics.

360 **Competing Interests**

361 The authors declare that they have no conflict of interest.

362 **Author Contribution**

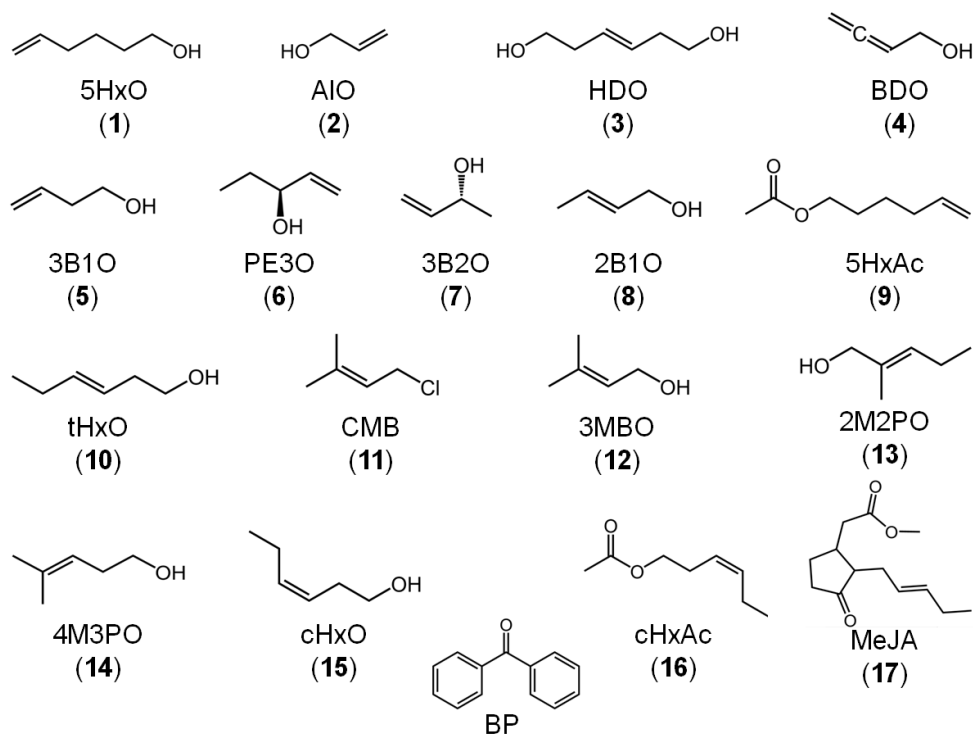
363 CA and RK conceptualized the research goals and designed the experiments. RK and JD
364 performed the laboratory work, while BH and DT planned and performed the computational
365 calculations. RK analyzed the experimental data and prepared the manuscript with contributions
366 from all co-authors, particularly BH, who wrote the sections on computational calculations and
367 prepared the corresponding figures. CA reviewed and edited the manuscript. CA and DT
368 provided oversight during the entire process.

369 **Data Availability**

370 Data are available upon request.

371 **Acknowledgements**

372 We thank Jacqueline R. Labins for assistance with rate constant measurements and Tran Nguyen
373 for helpful discussions on the reactivity of isoprene oxidation products. This research was funded
374 by the National Science Foundation (Grants AGS-1105049 and AGS-1649212), the University
375 of California - Davis Office of Graduate Studies, a UC Guru Gobind Singh Fellowship, and the
376 Agricultural and Environmental Chemistry Graduate Group at UC Davis.

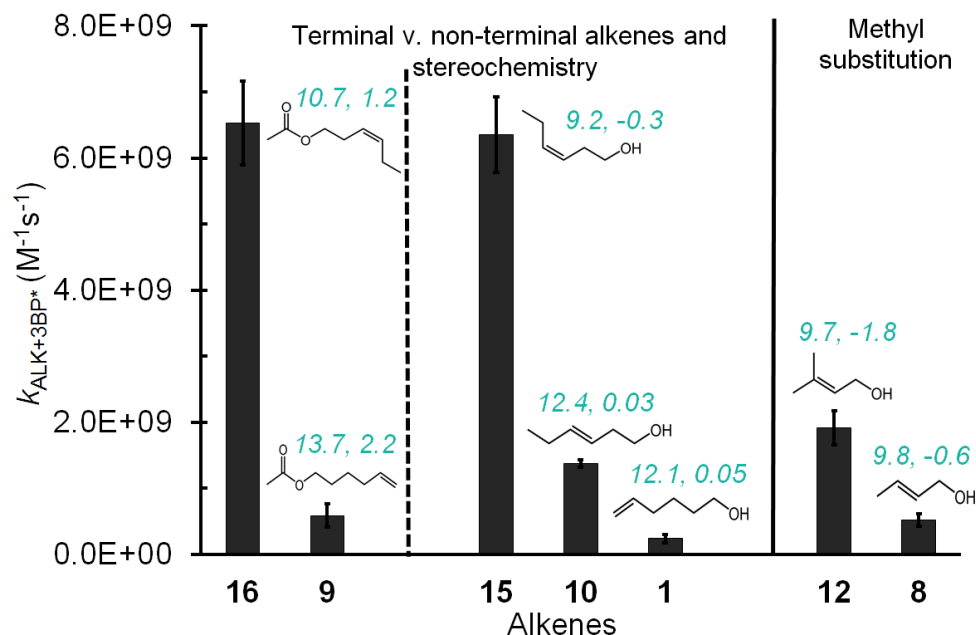


377

378

379

Fig. 1 Chemical structures of the reactant species used in this study: 17 alkenes and one model triplet, benzophenone. Compound numbers are in parentheses.



380

381

382 **Fig. 2** Comparison of three sets of alkenes to illustrate how rate constants with the benzophenone

383

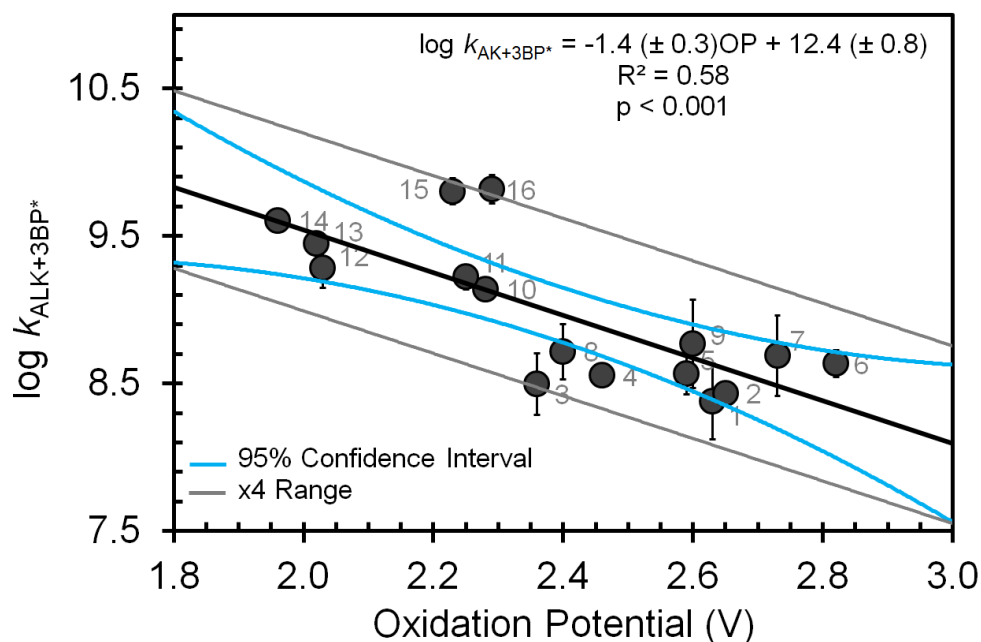
384

385

386

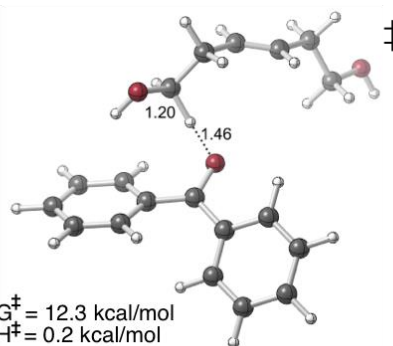
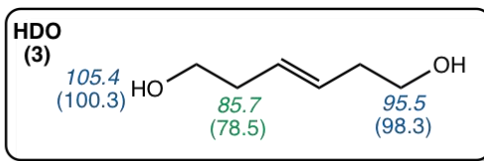
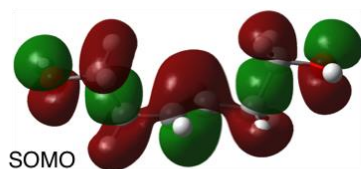
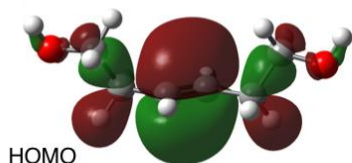
387

triplet state vary with double bond location, stereochemistry, and methyl substitution. The teal numbers on each alkene represent the lowest free energy (ΔG^\ddagger) and enthalpy (ΔH^\ddagger) transition state barriers in kcal mol $^{-1}$ for H-abstraction by triplet benzophenone; these were calculated at the uB3LYP/6-31+G(d,p) level of theory. Though computed barriers (Table 1) are not correlated with the overall rates measured, they broadly match the rate trends within a given set of alkenes in this figure.

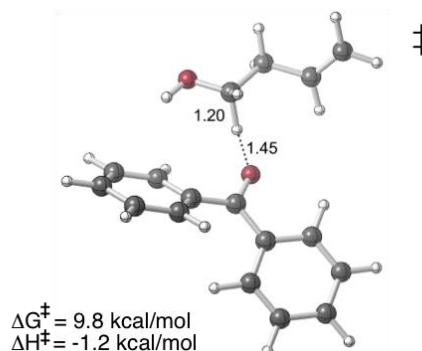
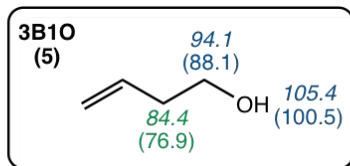
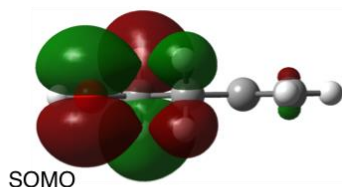
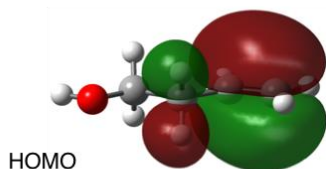


388

389 **Fig. 3** Correlation between measured bimolecular rate constants for alkenes with the triplet
390 excited state of benzophenone ($k_{\text{ALK}+3\text{BP}^*}$) and the computed one-electron oxidation potentials of
391 the alkenes. Numbers on each point represent the alkene numbers in Table 1. Blue lines represent
392 95 % confidence intervals of the regression prediction. The gray lines bound the region that is
393 within a factor of four of the regression prediction; all but one of the alkene values fall within
394 this. Methyl jasmonate (**17**) is not included in this figure due to computational challenges in
395 calculating its OP (see Table 1).

a) Electron removed from the π system

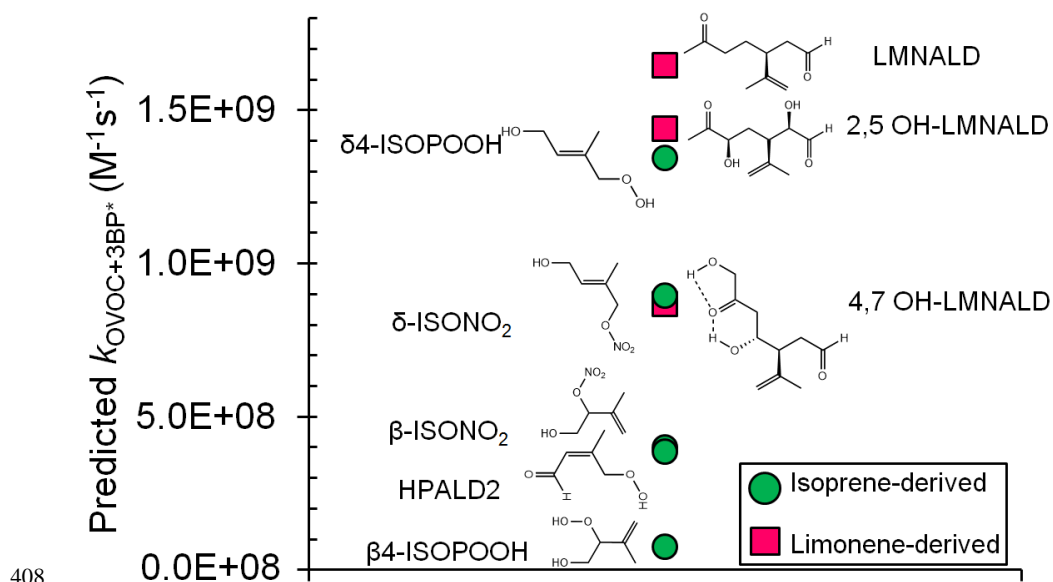
b) Electron removed from the oxygen



396

397

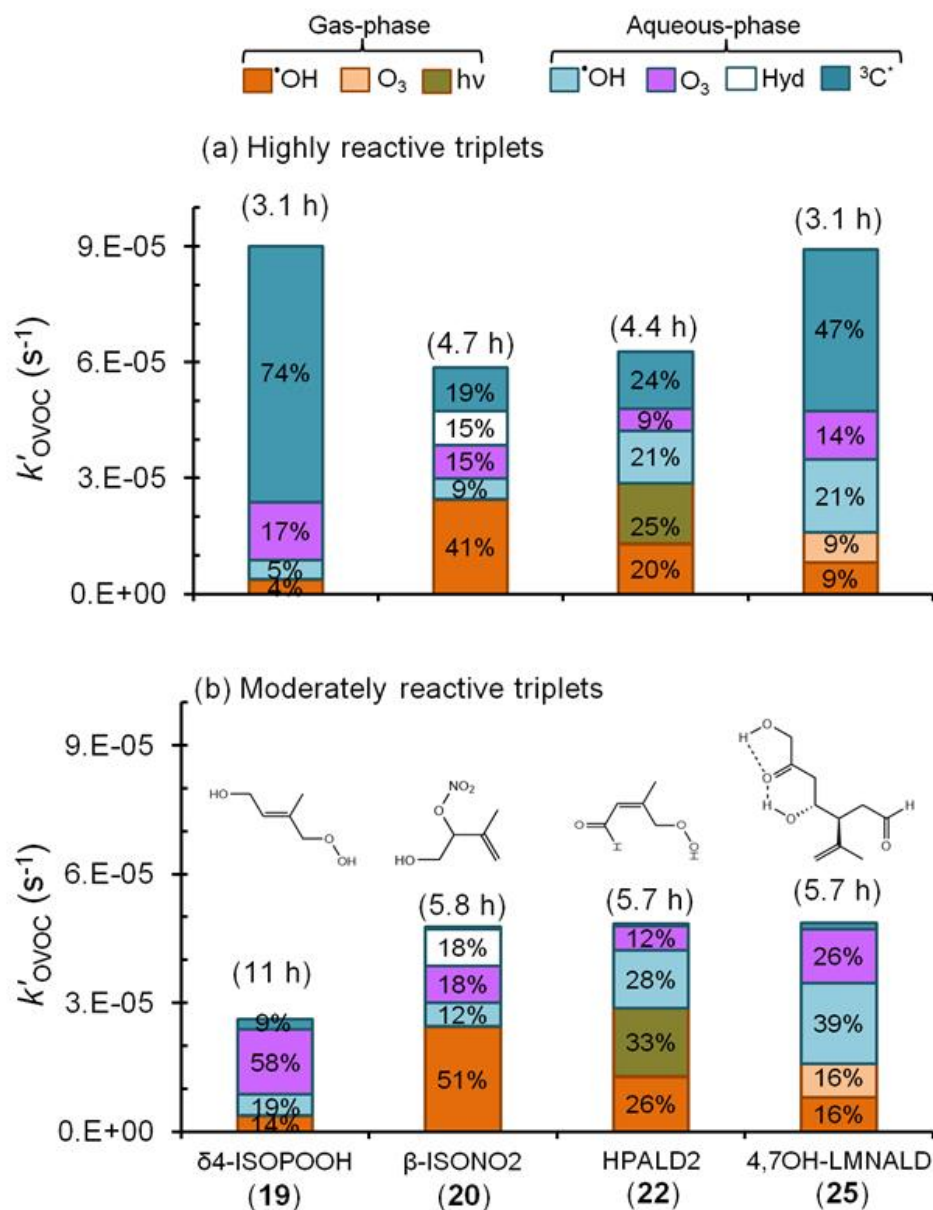
398 **Fig. 4** Diagrams of the highest occupied molecular orbitals (HOMOs) of the alkenes before
 399 oxidation, and the singly occupied molecular orbitals (SOMOs) after removal of one electron
 400 from the alkenes, and lowest energy transition state structures (\ddagger) of alkenes **3** and **5**. Bond
 401 dissociation enthalpy (italicized) and free energy (in parentheses) for various hydrogen atoms (in
 402 kcal mol⁻¹) for each alkene are shown in the boxes. Numbers in green are the lowest values, and
 403 thus represent the most labile hydrogen in each alkene. *a*) The electron removed during H-
 404 abstraction of HDO is predicted to come from the π system, but this results in delocalization due
 405 to hyperconjugation. *b*) The electron removed from 3B1O during H-abstraction is predicted to
 406 come from the oxygen. See SI Tables S2 and S3 for HOMO/SOMO structures and Fig. S4 for
 407 the bond dissociation enthalpies and free energies for other alkenes.



408

409

410 **Fig. 5** Predicted bimolecular rate constants for a range of limonene and isoprene oxidation
 411 products (OVOCs) with the triplet state of BP. Rate constants are estimated from the QSAR with
 412 one-electron oxidation potentials (OPs) (Fig. 3). Oxidation potentials used to predict the rate
 413 constants here (and in Table 1) are for the lowest energy isomers of the OVOCs, which are the
 414 structures shown here. The structures of some of the other, higher energy, isomers are shown in
 415 Table S4.



416

417 **Fig. 6** Estimated pseudo-first-order loss rate constants and corresponding lifetimes (in
 418 parentheses) for representative isoprene- and limonene-derived oxidation products in a foggy
 419 atmosphere (Tables S5–S7). Colors and data labels indicate the percentage of OVOC lost via
 420 each gas and aqueous pathway, including direct photoreaction ($h\nu$) and hydrolysis (Hyd);
 421 pathways contributing less than 4 % are not labeled. Panel (a) is a likely upper bound for the
 422 triplet contributions to OVOC loss where we assume that all fog triplets are highly reactive, like
 423 benzophenone. Panel (b) shows the more likely contribution from triplets, assuming moderately
 424 reactive triplets that are more representative of the average measured in fog waters and aqueous
 425 particle extracts (Kaur et al., 2018; Kaur and Anastasio, 2018) (Tables S5–S7).

426 **References**

- 427 Anastasio, C., Faust, B. C., and Allen, J. M.: Aqueous-phase photochemical formation of
428 hydrogen peroxide in authentic cloud waters, *Journal of Geophysical Research-*
429 *Atmospheres*, 99, 8231-8248, 1994.
- 430 Anastasio, C., Faust, B. C., and Rao, C. J.: Aromatic carbonyl compounds as aqueous-phase
431 photochemical sources of hydrogen peroxide in acidic sulfate aerosols, fogs, and clouds.
432 1. Non-phenolic methoxybenzaldehydes and methoxyacetophenones with reductants
433 (phenols), *Environmental science & technology*, 31, 218-232, 1996.
- 434 Anastasio, C., and McGregor, K. G.: Chemistry of fog waters in California's central valley: 1. In
435 situ photoformation of hydroxyl radical and singlet molecular oxygen, *Atmospheric*
436 *Environment*, 35, 1079-1089, 2001.
- 437 Arnold, W. A.: One electron oxidation potential as a predictor of rate constants of N-containing
438 compounds with carbonate radical and triplet excited state organic matter, *Environmental*
439 *Science: Processes & Impacts*, 16, 832-838, 2014.
- 440 Bahnmüller, S., von Gunten, U., and Canonica, S.: Sunlight-induced transformation of
441 sulfadiazine and sulfamethoxazole in surface waters and wastewater effluents, *Water*
442 *Research*, 57, 183-192, 2014.
- 443 Becke, A. D.: Density-functional thermochemistry. I. The effect of the exchange-only gradient
444 correction, *The Journal of chemical physics*, 96, 2155-2160, 1992.
- 445 Becke, A. D.: Becke's three parameter hybrid method using the LYP correlation functional, *J.*
446 *Chem. Phys.*, 98, 5648-5652, 1993.
- 447 Blando, J. D., and Turpin, B. J.: Secondary organic aerosol formation in cloud and fog droplets:
448 A literature evaluation of plausibility, *Atmospheric Environment*, 34, 1623-1632, 2000.
- 449 Boreen, A. L., Arnold, W. A., and McNeill, K.: Triplet-sensitized photodegradation of sulfa
450 drugs containing six-membered heterocyclic groups: identification of an SO₂ extrusion
451 photoproduct, *Environmental science & technology*, 39, 3630-3638, 2005.
- 452 Canonica, S., and Hoigné, J.: Enhanced oxidation of methoxy phenols at micromolar
453 concentration photosensitized by dissolved natural organic material, *Chemosphere*, 30,
454 2365-2374, 1995.
- 455 Canonica, S., Jans, U., Stemmler, K., and Hoigne, J.: Transformation kinetics of phenols in
456 water: Photosensitization by dissolved natural organic material and aromatic ketones,
457 *Environmental Science and Technology*, 29, 1822-1831, 1995.
- 458 Canonica, S., Hellrung, B., and Wirz, J.: Oxidation of phenols by triplet aromatic ketones in
459 aqueous solution, *Journal of Physical Chemistry A*, 104, 1226-1232, 2000.
- 460 Canonica, S., Hellrung, B., Müller, P., and Wirz, J.: Aqueous oxidation of phenylurea herbicides
461 by triplet aromatic ketones, *Environmental Science and Technology*, 40, 6636-6641,
462 2006a.
- 463 Canonica, S., Hellrung, B., Müller, P., and Wirz, J.: Aqueous oxidation of phenylurea herbicides
464 by triplet aromatic ketones, *Environmental science & technology*, 40, 6636-6641, 2006b.
- 465 Crouse, J. D., Paulot, F., Kjaergaard, H. G., and Wennberg, P. O.: Peroxy radical isomerization
466 in the oxidation of isoprene, *Physical Chemistry Chemical Physics*, 13, 13607-13613,
467 2011.
- 468 Erickson, P. R., Walpen, N., Guerard, J. J., Eustis, S. N., Arey, J. S., and McNeill, K.:
469 Controlling factors in the rates of oxidation of anilines and phenols by triplet methylene
470 blue in aqueous solution, *Journal of Physical Chemistry A*, 119, 3233-3243, 2015.
- 471 Finlayson-Pitts, B. J., and Pitts Jr, J. N.: Chemistry of the Upper and Lower Atmosphere:
472 Theory, Experiments, and Applications, Academic press, 1999.



- 473 Frisch, M., Trucks, G., Schlegel, H. B., Scuseria, G., Robb, M., Cheeseman, J., Scalmani, G.,
474 Barone, V., Mennucci, B., and Petersson, G.: Gaussian 09, revision a. 02, gaussian, Inc.,
475 Wallingford, CT, 200, 2009.
- 476 Fu, H., Ciuraru, R., Dupart, Y., Passananti, M., Tinel, L., Rossignol, S. p., Perrier, S., Donaldson,
477 D. J., Chen, J., and George, C.: Photosensitized production of atmospherically reactive
478 organic compounds at the air/aqueous interface, *Journal of the American Chemical*
479 *Society*, 137, 8348-8351, 2015.
- 480 Gelencsér, A., and Varga, Z.: Evaluation of the atmospheric significance of multiphase reactions
481 in atmospheric secondary organic aerosol formation, *Atmospheric Chemistry and*
482 *Physics*, 5, 2823-2831, 2005.
- 483 Hallquist, M., Wenger, J., Baltensperger, U., Rudich, Y., Simpson, D., Claeys, M., Dommen, J.,
484 Donahue, N., George, C., and Goldstein, A.: The formation, properties and impact of
485 secondary organic aerosol: current and emerging issues, *Atmospheric Chemistry and*
486 *Physics*, 9, 5155-5236, 2009.
- 487 Herrmann, H., Hoffmann, D., Schaefer, T., Brüner, P., and Tilgner, A.: Tropospheric aqueous-
488 phase free-radical chemistry: Radical sources, spectra, reaction kinetics and prediction
489 tools, *ChemPhysChem*, 11, 3796-3822, 2010.
- 490 Herrmann, H., Schaefer, T., Tilgner, A., Styler, S. A., Weller, C., Teich, M., and Otto, T.:
491 Tropospheric aqueous-phase chemistry: Kinetics, mechanisms, and its coupling to a
492 changing gas phase, *Chemical Reviews*, 115, 4259-4334, 2015.
- 493 Jacobs, M. I., Burke, W., and Elrod, M. J.: Kinetics of the reactions of isoprene-derived
494 hydroxynitrates: gas phase epoxide formation and solution phase hydrolysis,
495 *Atmospheric Chemistry and Physics*, 14, 8933-8946, 2014.
- 496 Kaur, R., and Anastasio, C.: Light absorption and the photoformation of hydroxyl radical and
497 singlet oxygen in fog waters, *Atmospheric Environment*, 164, 387-397, 2017.
- 498 Kaur, R., and Anastasio, C.: First Measurements of Organic Triplet Excited States in
499 Atmospheric Waters, *Environmental science & technology*, 52, 5218-5226, 2018.
- 500 Kaur, R., Labins, J. R., Helbock, S. S., Jiang, W., K.J., B., Zhang, Q., and Anastasio, C.:
501 Photooxidants from Brown Carbon and Other Chromophores in Illuminated Particle
502 Extracts, *In Preparation*, 2018.
- 503 Khamaganov, V. G., and Hites, R. A.: Rate Constants for the Gas-Phase Reactions of Ozone
504 with Isoprene, α - and β -Pinene, and Limonene as a Function of Temperature, *The Journal*
505 *of Physical Chemistry A*, 105, 815-822, 2001.
- 506 Kroll, J. H., and Seinfeld, J. H.: Chemistry of secondary organic aerosol: Formation and
507 evolution of low-volatility organics in the atmosphere, *Atmospheric Environment*, 42,
508 3593-3624, 2008.
- 509 Laskin, A., Laskin, J., and Nizkorodov, S. A.: Chemistry of atmospheric brown carbon,
510 *Chemical Reviews*, 115, 4335-4382, 2015.
- 511 Lee, A. K., Herckes, P., Leitch, W., Macdonald, A., and Abbatt, J.: Aqueous OH oxidation of
512 ambient organic aerosol and cloud water organics: Formation of highly oxidized
513 products, *Geophysical Research Letters*, 38, 2011.
- 514 Lee, C., Yang, W., and Parr, R. G.: Development of the Colle-Salvetti correlation-energy
515 formula into a functional of the electron density, *Physical review B*, 37, 785, 1988.
- 516 Lee, L., Teng, A. P., Wennberg, P. O., Crounse, J. D., and Cohen, R. C.: On Rates and
517 Mechanisms of OH and O₃ Reactions with Isoprene-Derived Hydroxy Nitrates, *The*
518 *Journal of Physical Chemistry A*, 118, 1622-1637, 2014.
- 519 Legault, C.: CYLview, 1.0 b, Université de Sherbrooke, 2009.



- 520 Li, W.-Y., Li, X., Jockusch, S., Wang, H., Xu, B., Wu, Y., Tsui, W. G., Dai, H.-L., McNeill, V.
521 F., and Rao, Y.: Photoactivated production of secondary organic species from isoprene in
522 aqueous systems, *The Journal of Physical Chemistry A*, 120, 9042-9048, 2016.
- 523 Lim, Y., Tan, Y., Perri, M., Seitzinger, S., and Turpin, B.: Aqueous chemistry and its role in
524 secondary organic aerosol (SOA) formation, *Atmospheric Chemistry and Physics*, 10,
525 10521-10539, 2010.
- 526 Marais, E. A., Jacob, D. J., Jimenez, J. L., Campuzano-Jost, P., Day, D. A., Hu, W., Krechmer,
527 J., Zhu, L., Kim, P. S., and Miller, C. C.: Aqueous-phase mechanism for secondary
528 organic aerosol formation from isoprene: application to the southeast United States and
529 co-benefit of SO₂ emission controls, *Atmospheric Chemistry and Physics*, 16, 1603-
530 1618, 2016.
- 531 Marenich, A. V., Cramer, C. J., and Truhlar, D. G.: Universal solvation model based on the
532 generalized Born approximation with asymmetric descreening, *Journal of chemical*
533 *theory and computation*, 5, 2447-2464, 2009.
- 534 Mayer, P. M., Parkinson, C. J., Smith, D. M., and Radom, L.: An assessment of theoretical
535 procedures for the calculation of reliable free radical thermochemistry: A recommended
536 new procedure, *The Journal of chemical physics*, 108, 604-615, 1998.
- 537 Montgomery Jr, J. A., Frisch, M. J., Ochterski, J. W., and Petersson, G. A.: A complete basis set
538 model chemistry. VI. Use of density functional geometries and frequencies, *The Journal*
539 *of chemical physics*, 110, 2822-2827, 1999.
- 540 Ng, N., Kwan, A., Surratt, J., Chan, A., Chhabra, P., Sorooshian, A., Pye, H. O., Crouse, J.,
541 Wennberg, P., and Flagan, R.: Secondary organic aerosol (SOA) formation from reaction
542 of isoprene with nitrate radicals (NO₃), *Atmospheric Chemistry and Physics*, 8, 4117-
543 4140, 2008.
- 544 Paulot, F., Crouse, J., Kjaergaard, H., Kroll, J., Seinfeld, J., and Wennberg, P.: Isoprene
545 photooxidation: new insights into the production of acids and organic nitrates,
546 *Atmospheric Chemistry and Physics*, 9, 1479-1501, 2009a.
- 547 Paulot, F., Crouse, J. D., Kjaergaard, H. G., Kürten, A., Clair, J. M. S., Seinfeld, J. H., and
548 Wennberg, P. O.: Unexpected epoxide formation in the gas-phase photooxidation of
549 isoprene, *Science*, 325, 730-733, 2009b.
- 550 Petersson, G., Bennett, A., Tensfeldt, T. G., Al-Laham, M. A., Shirley, W. A., and Mantzaris, J.:
551 A complete basis set model chemistry. I. The total energies of closed-shell atoms and
552 hydrides of the first-row elements, *The Journal of chemical physics*, 89, 2193-2218,
553 1988.
- 554 Petersson, G., and Al-Laham, M. A.: A complete basis set model chemistry. II. Open-shell
555 systems and the total energies of the first-row atoms, *The Journal of chemical physics*,
556 94, 6081-6090, 1991.
- 557 Petersson, G., Tensfeldt, T. G., and Montgomery Jr, J.: A complete basis set model chemistry.
558 III. The complete basis set-quadratic configuration interaction family of methods, *The*
559 *Journal of chemical physics*, 94, 6091-6101, 1991.
- 560 Richards-Henderson, N. K., Pham, A. T., Kirk, B. B., and Anastasio, C.: Secondary Organic
561 Aerosol from Aqueous Reactions of Green Leaf Volatiles with Organic Triplet Excited
562 States and Singlet Molecular Oxygen, *Environmental science & technology*, 49, 268-276,
563 2014a.
- 564 Richards-Henderson, N. K., Pham, A. T., Kirk, B. B., and Anastasio, C.: Secondary organic
565 aerosol from aqueous reactions of green leaf volatiles with organic triplet excited states
566 and singlet molecular oxygen, *Environmental Science and Technology*, 49, 268-276,
567 2014b.



- 568 Rossignol, S. p., Aregahegn, K. Z., Tinel, L., Fine, L., Nozière, B., and George, C.: Glyoxal
569 induced atmospheric photosensitized chemistry leading to organic aerosol growth,
570 Environmental science & technology, 48, 3218-3227, 2014.
- 571 Schöne, L., and Herrmann, H.: Kinetic measurements of the reactivity of hydrogen peroxide and
572 ozone towards small atmospherically relevant aldehydes, ketones and organic acids in
573 aqueous solutions, Atmospheric Chemistry and Physics, 14, 4503, 2014.
- 574 Smith, J. D., Sio, V., Yu, L., Zhang, Q., and Anastasio, C.: Secondary organic aerosol production
575 from aqueous reactions of atmospheric phenols with an organic triplet excited state,
576 Environmental Science and Technology, 48, 1049-1057, 2014.
- 577 St. Clair, J. M., Rivera-Rios, J. C., Crouse, J. D., Knap, H. C., Bates, K. H., Teng, A. P.,
578 Jørgensen, S., Kjaergaard, H. G., Keutsch, F. N., and Wennberg, P. O.: Kinetics and
579 Products of the Reaction of the First-Generation Isoprene Hydroxy Hydroperoxide
580 (ISOPOOH) with OH, The Journal of Physical Chemistry A, 120, 1441-1451, 2015.
- 581 Stephens, P., Devlin, F., Chabalowski, C., and Frisch, M. J.: Ab initio calculation of vibrational
582 absorption and circular dichroism spectra using density functional force fields, The
583 Journal of Physical Chemistry, 98, 11623-11627, 1994.
- 584 Surratt, J. D., Murphy, S. M., Kroll, J. H., Ng, N. L., Hildebrandt, L., Sorooshian, A.,
585 Szmigielski, R., Vermeylen, R., Maenhaut, W., and Claeys, M.: Chemical composition of
586 secondary organic aerosol formed from the photooxidation of isoprene, The Journal of
587 Physical Chemistry A, 110, 9665-9690, 2006.
- 588 Tirado-Rives, J., and Jorgensen, W. L.: Performance of B3LYP density functional methods for a
589 large set of organic molecules, Journal of Chemical Theory and Computation, 4, 297-306,
590 2008.
- 591 Tsui, W. G., Rao, Y., Dai, H.-L., and McNeill, V. F.: Modeling photosensitized secondary
592 organic aerosol formation in laboratory and ambient aerosols, Environmental Science and
593 Technology, 51, 7496-7501, 2017.
- 594 US EPA. Estimation Programs Interface Suite™ for Microsoft® Windows v 4.1: Estimation
595 Programs Interface Suite™ for Microsoft® Windows, v 4.1. United States Environmental
596 Protection Agency, Washington, DC, USA., 2016.
- 597 Volkamer, R., Ziemann, P., and Molina, M.: Secondary organic aerosol formation from
598 acetylene (C₂H₂): seed effect on SOA yields due to organic photochemistry in the
599 aerosol aqueous phase, Atmospheric Chemistry and Physics, 9, 1907-1928, 2009.
- 600 Walser, M. L., Desyaterik, Y., Laskin, J., Laskin, A., and Nizkorodov, S. A.: High-resolution
601 mass spectrometric analysis of secondary organic aerosol produced by ozonation of
602 limonene, Physical Chemistry Chemical Physics, 10, 1009-1022, 2008.
- 603 Warren, J. J., Tronic, T. A., and Mayer, J. M.: Thermochemistry of proton-coupled electron
604 transfer reagents and its implications, Chemical Reviews, 110, 6961-7001, 2010.
- 605 Wilkinson, F., Helman, W. P., and Ross, A. B.: Rate constants for the decay and reactions of the
606 lowest electronically excited singlet-state of molecular-oxygen in solution - an expanded
607 and revised compilation, Journal of Physical and Chemical Reference Data, 24, 663-
608 1021, 1995.
- 609 Wolfe, G. M., Crouse, J. D., Parrish, J. D., Clair, J. M. S., Beaver, M. R., Paulot, F., Yoon, T.
610 P., Wennberg, P. O., and Keutsch, F. N.: Photolysis, OH Reactivity and Ozone Reactivity
611 of a Proxy for Isoprene-Derived Hydroperoxyenals (HPALDs), Physical Chemistry
612 Chemical Physics, 14, 7276-7286, 2012.
- 613 Yu, L., Smith, J., Laskin, A., Anastasio, C., Laskin, J., and Zhang, Q.: Chemical characterization
614 of SOA formed from aqueous-phase reactions of phenols with the triplet excited state of



- 615 carbonyl and hydroxyl radical, *Atmospheric Chemistry and Physics*, 14, 13801-13816,
616 2014.
- 617 Zepp, R. G., Wolfe, N. L., Baughman, G. L., and Hollis, R. C.: Singlet oxygen in natural waters,
618 *Nature*, 267, 421-423, 1977.
- 619 Zhang, Q., Jimenez, J. L., Canagaratna, M. R., Allan, J. D., Coe, H., Ulbrich, I., Alfarra, M. R.,
620 Takami, A., Middlebrook, A. M., Sun, Y. L., Dzepina, K., Dunlea, E., Docherty, K.,
621 DeCarlo, P. F., Salcedo, D., Onasch, T., Jayne, J. T., Miyoshi, T., Shimojo, A.,
622 Hatakeyama, S., Takegawa, N., Kondo, Y., Schneider, J., Drewnick, F., Borrmann, S.,
623 Weimer, S., Demerjian, K., Williams, P., Bower, K., Bahreini, R., Cottrell, L., Griffin, R.
624 J., Rautiainen, J., Sun, J. Y., Zhang, Y. M., and Worsnop, D. R.: Ubiquity and dominance
625 of oxygenated species in organic aerosols in anthropogenically-influenced northern
626 hemisphere midlatitudes, *Geophysical Research Letters*, 34, n/a-n/a, 2007.
- 627



628 **Table 1.** Measured alkene-benzophenone triplet reaction rate constants, predicted OVOC-
 629 benzophenone triplet reaction rate constants, and computed parameters for the alkenes.

#	Name	Abbreviation	OP ^a (V)	ΔG^\ddagger ^b (kcal mol ⁻¹)	ΔH^\ddagger ^c (kcal mol ⁻¹)	Measured $k_{\text{ALK}+\text{3BP}^*}$ ^d (10 ⁸ M ⁻¹ s ⁻¹)
Alkenes						
1	5-Hexen-1-ol	5HxO	2.63	12.1	0.05	2.4 (0.6)
2	2-Propen-1-ol (Allyl alcohol)	AlO	2.65	10.8	-0.04	2.7 (0.2)
3	3-Hexene-1,6-diol	HDO	2.36	12.3	0.2	3.1 (0.7)
4	2,3-Butadien-1-ol	BDO	2.46	10.5	-1.5	3.6 (0.3)
5	3-Buten-1-ol	3B1O	2.59	9.8	-1.2	3.7 (0.5)
6	1-Penten-3-ol	PE3O	2.82	11.3	-1.0	4.3 (0.4)
7	3-Buten-2-ol	3B2O	2.73	10.6	-1.0	4.9 (1.3)
8	2-Buten-1-ol	2B1O	2.40	9.8	-0.6	5.2 (1.0)
9	5-Hexenyl acetate	5HxAc	2.60	13.7	2.2	5.9 (1.8)
10	trans-3-hexen-1-ol	tHxO	2.28	12.4	0.03	14 (1)
11	1-Chloro-3-methyl-2-butene	CMB	2.25	14.1	2.7	17 (1) ^e
12	3-Methyl-2-buten-1-ol (Prenol)	3MBO	2.03	9.7	-1.8	19 (3)
13	2-Methyl-2-penten-1-ol	2M2PO	2.02	11.6	-1.4	28 (1)
14	4-Methyl-3-penten-1-ol	4M3PO	1.96	11.5	-0.4	40 (2)
15	cis-3-Hexen-1-ol	cHxO	2.23	9.2	-0.3	64 (6)
16	cis-3-Hexenyl acetate	cHxAc	2.29	10.7	1.2	65 (6)
17	Methyl jasmonate	MeJA	- ^f	- ^f	- ^f	75 (5)
Predictions for isoprene- and limonene-derived OVOCs						Predicted $k_{\text{OVOC}+\text{3BP}^*}$ ^g (10 ⁸ M ⁻¹ s ⁻¹)
18	β 4-Isoprene hydroxyhydroperoxide	β 4- ISOPOOH	3.13	13.2	0.3	0.80 (0.18)
19	δ 4-Isoprene hydroxyhydroperoxide	δ 4- ISOPOOH	2.28	10.5	-2.0	14 (3)
20	β -Isoprene hydroxynitrate	β -ISONO2	2.64	13.2	1.4	4.1 (0.9)
21	δ -Isoprene hydroxynitrate	δ -ISONO2	2.40	10.0	-1.9	9.2 (2.1)
22	Isoprene hydroperoxyaldehyde 2	HPALD2	2.65	10.4	-2.6	4.0 (0.9)
23	Limononaldehyde	LMNALD	2.22	9.9	-1.4	17 (4)
24	2,5-Dihydroxy limononaldehyde	2,5OH- LMNALD	2.26	10.1	-2.2	15 (3)
25	4,7-Dihydroxy limononaldehyde	4,7-OH- LMNALD	2.41	10.6	-0.8	8.9 (2.0)

630 ^a One-electron oxidation potential, calculated using the CBS-QB3 compound method.

631 ^{b,c} Lowest transition state energy barrier for H-abstraction by triplet benzophenone, calculated using
 632 uB3LYP/6-31+G(d,p).

633 ^d Measured bimolecular rate constant for alkene reacting with ³BP* with uncertainties of ± 1 standard
 634 deviation, determined from triplicate measurements (Table S1 of the supplement).



635 ^e Listed uncertainty is ± 1 standard error, $n=1$.

636 ^f The oxidation potential and energy barriers could not be computed for MeJA (**17**). Because the CB3-
637 QB3 method scales at N^7 (where N is the number of atoms), the larger compound required more
638 computational power than available.

639 ^g Predicted bimolecular rate constant for select isoprene- and limonene-derived OVOCs reacting with
640 ³BP*, determined from the correlation between OP and $k_{\text{ALK}+3\text{BP}^*}$. Listed uncertainties are ± 1 standard
641 error propagated from the error of the slope of the quantitative structure-activity relationship between
642 oxidation potential and $k_{\text{ALK}+3\text{BP}^*}$ (Fig. 3).